Research Square

Preprints are preliminary reports that have not undergone peer review.
They should not be considered conclusive, used to inform clinical practice,
or referenced by the media as validated information.

DFT insights into structural, electronic and optical characteristics of undoped and Sc-doped GeO2 rutile

Beloufa Nabil

n.beloufa@ihfr.edu.dz

Hydrometeorological Institute for Training and Research IHFR

Kebaili Aboubakr Seddik

Hassiba Benbouali University of Chlef

Drief Mohammed

Djillali Liabes University

Ouled Ali Mohamed

University of Ahmed Draia

Bekheira Samir

National Polytechnic School Oran, ENPO-MA

Boualem Kada

University of AinTemouchent

Research Article

Keywords: Density functional theory, FP-LAPW, Sc doped r-GeO2, optical properties

Posted Date: August 18th, 2026

DOI: https://doi.org/10.21203/rs.3.rs-10647058/v1

License: This work is licensed under a Creative Commons Attribution 4.0 International License.
Read Full License

Additional Declarations: No competing interests reported.

Version of Record: A version of this preprint was published at Chemical Papers on September 10th, 2026. See the published version at https://doi.org/10.1007/s11696-026-05595-7.

DFT insights into structural, electronic and optical characteristics of undoped and Sc-doped GeO_2 rutile

Beloufa Nabil [a, b *], Kebaili Aboubakr Seddik [c], Drief Mohammed [d], Ouled Ali Mohamed[e], Bekheira Samir [b,f], Boualem Kada [g]

[a] *Hydrometeorological Institute for Training and Research IHFR, Ibnou Rochd.Bp 7019,Oran Algeria*

[b] *National Polytechnic School Oran, Laboratory of Micro and Nanophysics, ENPO-MA, BP 1523, Oran, Algeria*

[c] *Department of Physics, Faculty of Exact Sciences and Informatics, Hassiba Benbouali University of Chlef, 02000, Chlef, Algeria*

[d] *Magnetic Materials Laboratory, Faculty of Exact Sciences, Djillali Liabes University, Sidi Bel-Abbes, Algeria*

[e] *Faculty of Matter Sciences, Mathematics and Computer Sciences , University of Ahmed Draia, Adrar, Algeria.*

[f] *Higher Normal School of Kouba* B.P N°92 16308 Kouba – Alger*, Algeria*

[g] *Materials Science and Applications Laboratory (LSMA), Faculty of Sciences and Technology, University of AinTemouchent, Belhadj Bouchaib.BP 284, Ain-Temouchent, 46000, Algeria*

Abstract

Wide-bandgap materials have shown promising potential for optoelectronic devices, due to their high transparency, excellent thermal and chemical resistance, and favorable electron mobility. In this study, density functional theory (DFT) calculations using ab initio modeling were employed to examine the structural and optoelectronic characteristics of germanium dioxide (GeO_2) in its rutile phase substituted with scandium ($Sc_xGe_{1-x}O_2$, where x = 0, 0.0416, 0.0625, 0.0832, and 0.125). The calculated formation energies are negative, indicating that these materials remain thermodynamically stable. It is observed that only the addition of the Sc dopant induces changes in the structural behavior of r-GeO_2, such as an increase in the lattice parameters.

The band gap of pure r-GeO_2 is 4.112 eV at ($\Gamma - \Gamma$), by using the Trans-Blaha-modified Becke-Johnson (TB-mBJ) approach. This value decreases to 3.778 eV as the Sc content increases, and due to the 3d orbitals of Sc, the Fermi level shifts toward the valence band, introducing holes, which leads to p-type conduction. The partial density of states (PDOS) clearly shows that the Sc-3d states are induced by the replacement of Ge with Sc, resulting in a reduction of the bandgap. The optical spectra, including the real and imaginary parts, light absorption, optical reflectivity, conductivity, refractive index, extinction coefficient, and energy loss spectrum, were studied. Furthermore, these

optical properties are improved after doping with scandium compared to those of pure r-GeO_2. On the other hand, due to the high optical conductivity and absorption in the UV region, this demonstrates that Sc-doped r-GeO_2 is an interesting candidate for advanced optoelectronic devices and UV detection.

Keywords: Density functional theory; FP-LAPW; Sc doped r-GeO_2 ; optical properties

Introduction

Wide-bandgap (WBG) semiconductors are defined by a bandgap (Eg) greater than that of conventional semiconductors, specifically higher than 3.4 eV [1]. These materials are used in various fields, including light-emitting diodes, short-wavelength lasers [2], and power devices [3]. Germanium(IV) dioxide is an inorganic compound with the chemical formula GeO_2 [4, 5].In its three-dimensional form, it exists in crystalline, liquid, and amorphous states. The most stable structures at room temperature are the trigonal or hexagonal quartz phases ($P3_121$, $D4^3$), analogous to α- quartz of SiO_2 [6], the tetragonal rutile-type structure ($P4_2/mnm$, $D1^4h$), and the amorphous structure [7– 9].

The rutile structure of GeO_2 has a tetragonal bravais lattice, with a = 4.4066 Å and c = 2.8619 Å [10]. This phase is thermodynamically stable at temperatures reaching 1300 °C [11], has high chemical resistance [12], and high density [13]. It also shows chemical and structural similarities with other oxides, such as SnO_2 and TiO_2, which also crystallize in the rutile phase [14–16]. At room temperature, GeO_2 adopts a tetragonal structure, the densest and most thermodynamically stable phase, before transforming into a less dense hexagonal phase at 1306 K [17]. GeO_2 is a wide-bandgap semiconductor (Eg = 4.68 eV) [4, 18], corresponding to the UVC region (200 nm–290 nm) [19]. it has significant electron 300 $cm^2/V{\cdot}s$ and carrier mobility 30 $cm^2/V{\cdot}$[20]. Experiments show a direct band gap [21]. This material exhibits remarkable thermal, optical, and electrical properties, including high thermal stability [22], excellent light transmission in the 280–5000 nm range [23], high dielectric constant and refractive index [24], and also a reduced supply voltage [25, 26].Due to these properties, GeO_2 is a promising candidate for various optical, electronic, and semiconductor applications, such as solar cells, Li-ion batteries [27, 28], and optical fibers [11], as well as for physical and chemical applications, notably the fabrication of high-photorefractive planar waveguides [29, 30].

Transition metal doping is an efficient method for changing the material's physical properties [31]. However, wide-bandgap (WBG) semiconductors are characterized by high donor ionization energies, which makes symmetric doping particularly difficult [32]. In contrast, GeO_2 is capable of n and p-type doping due to the dopant ionization energies, which are lower than those typically observed in WBG semiconductors [20]. r-GeO_2 thus emerges as a promising candidate to address the shortage of p-type transparent conductive oxides (TCOs) [33]. By comparison, widely studied oxides such as TiO_2 and SnO_2 exhibit significant limitations for p-type doping [34]. The discovery of new transparent conductive oxides has sparked growing interest, particularly in yttrium (Y) and scandium (Sc), [35]. Boujnah et al. [36] revealed that 3d transition metals doped r-SnO_2 form p-type transparent conductive oxides that are excellent for solar cells. TiO_2 doped with yttrium (Y) proved effective in improving photocatalytic activity and extending the absorption range towards visible light [37]. However, the impact of certain specific dopants, particularly transition metals, on material

properties remains poorly understood. In this context, scandium (Sc) was chosen as a dopant because it can promote p-type doping, modulate electronic properties, and preserve the stability of GeO_2 due to its unique electronic characteristics and influence on the material's electronic structure. Additionally, the ionic size of Sc^{3+}, which is compatible with the rutile structure of GeO_2, enables effective doping while maintaining the integrity of the crystal lattice. According to Qodziana et al. [38], GeO_2 undergoes several phase transitions under high pressure: rutile → $CaCl_2$ at 19 GPa → a-PbO_2 at 36 GPa → pyrite (Pa-3) at 65.5 GPa. Chae et al. [26] showed that when aluminum replaces Ge at the site, it can act as a potential acceptor with relatively high ionization energies ranging from 0.45 to 0.54 eV. Samanta et al. [39] further demonstrated that lattice parameters strongly influence the bandgap width of r-GeO_2 calculated by DFT. To study the physical properties of GeO_2, several theoretical methods were employed, including FP-LAPW [28], GGA with finite electric field application [40], the GIPAW approach using the CASTEP code [41], the local density approximation with plane waves, and the two-center strong-coupling method [42]. Recently, it was observed that replacing GeO_2 with yttrium oxide-doped GeO_2 (Y-GeO_2) significantly improved the water resistance of the Y-GeO_2/Ge cell [43]. This improvement was mainly attributed to the modification of the GeO_2 structure by the incorporation of the Y^{3+} cation [44]. However, to our knowledge, most theoretical work on r-GeO_2 is limited to the density functional theory (DFT) approach, which is known to underestimate the bandgap width. Furthermore, to date, no systematic study has been published on scandium-doped GeO_2 (a transition metal), particularly regarding its structural, electronic, and optical properties.

The main objective of this study is to examine the influence of p-type doping with this 3d transition metal on the physical properties of pure and Sc doped r-GeO_2 at various concentrations (x = 4.16%, 6.25%, and 12.5%). In the organization of this article, we describe the computational method used within the theoretical framework (second section), then we give in the third part the main results related to geometry, as well as the optoelectronics properties. The final section provides the general conclusions drawn from the main results.

Computational methodology

The WIEN2k code [45] is used to calculate the properties of germanium oxide in both its pure rutile phase and when doped with scandium ($Sc_xGe_{1-x}O_2$, where x = 0, 4.16%, 6.25%, 8.32%, and 12.5%) which include structural and optoelectronic properties. By using the FP-LAPWmethod [46], based on density functional theory (DFT) [47, 48]. The exchange-correlation potential was treated using the generalized gradient approximation (GGA) [49] with the Perdew-Burke-Ernzerhof (PBE) parameterization. These functionals improve the description of structural properties compared to standard DFT approaches and provide corrections for better accounting of electronic interactions. The Tran-Blaha-modified Becke-Johnson (TB-mBJ) was applied to calculate the optoelcetronic properties of this compounds [50], allowing for a more accurate estimation of the bandgap. The radius values were set at 1.86 a.u, 1.89 a.u, and 1.68 a.u for Ge, Sc, and O atoms, respectively. These values are essential for defining the size of the muffin-tin spheres and were chosen to prevent any overlap. The cutoff parameter was set to ensure convergence, with $K_{max} \times RMT = 7$, allowing control over calculation accuracy while limiting computation time. Inside the spheres, the maximum value of the spherical harmonics was set to $l_{max} = 8$ to ensure an accurate description of the electronic wave

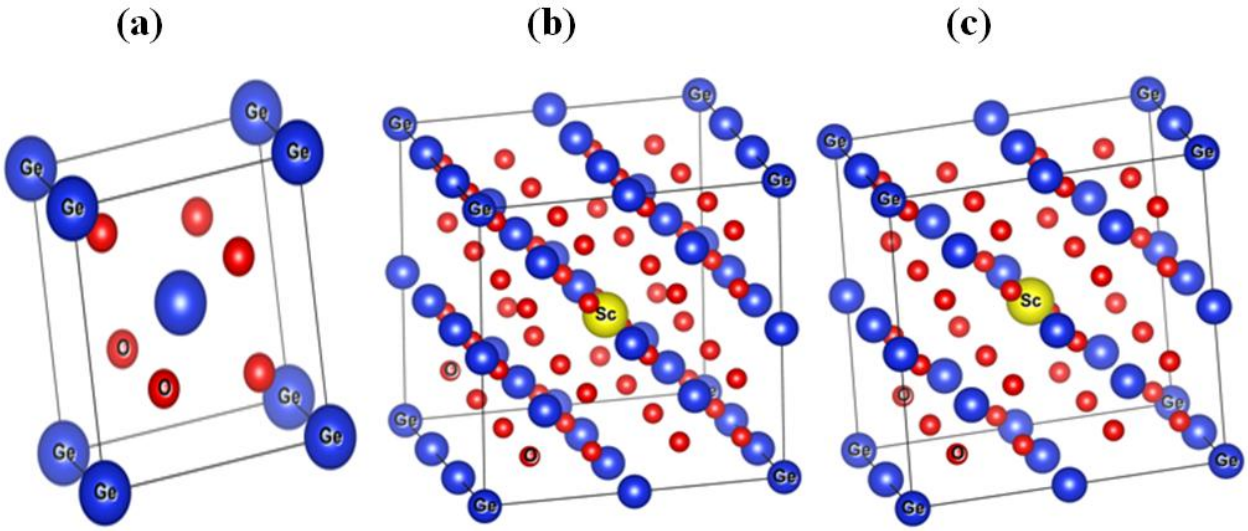
functions in the valence region. In addition, the Fourier expansion parameter, referred to as "Gmax," which corresponds to the maximum reciprocal vector of the lattice involved in the detailed description of the charge density, is set at G_{max} = 12.0 a.u.$^{-1}$., ensuring satisfactory convergence of the electronic calculations. The energy cutoff, which determines the division between the core and valence electronic states, is set at a value of -9 Ry .

The iteration is continued until the total energy reaches stability at 10^{-4} Ry and 10^{-3} e for charge, and the integration over the first Brillouin zone was performed using a Monkhorst–Pack grid with dimensions of 8 × 8 × 12 for pure r-GeO_2 and 7 × 7 × 7 for the doped systems [51]. The energy band structures were calculated along the principal directions Γ–X–M–Γ–Z–R–A–Z of the first Brillouin zone using the GGA-PBE and TB-mBJ approximations. The valence electron configurations of the atoms are as follows: Ge: [Ar] $3d^{10}$ $4s^2$ $4p^2$, Sc: [Ar] $3d^1$ $4s^2$, and O: [He] $2s^2$ $2p^4$. The optical properties were evaluated by applying a scissor correction with an amplitude of 1.0 eV.

Structural optimization

Rutile Germanium oxide (r-GeO_2) has a tetragonal crystal structure with the space group $P4_2/mnm$ (No. 136) [52] and exhibits D_4h^{14} local symmetry (Fig. 1-a). The conventional structure consists two types of atoms: germanium (Ge) and oxygen (O), with germanium cations occupying the Wyckoff sites 2a (0, 0, 0) and (1/2, 1/2, 1/2) while the oxygen anions are placed in position 4f sites: (u, u, 0), (1− u, 1− u, 0), (½+ u, ½ − u, ½), (½ − u, ½ +u, ½), and u = 0.306.

The optimized lattice constants for r-GeO_2 in the rutile phase are: a = b = 4.398 Å and c = 2.863 Å. This data is consistent with experimental results [10] and other theoretical calculations [28,53,54], which attests that the calculations are precise enough and the data obtained are reliable.



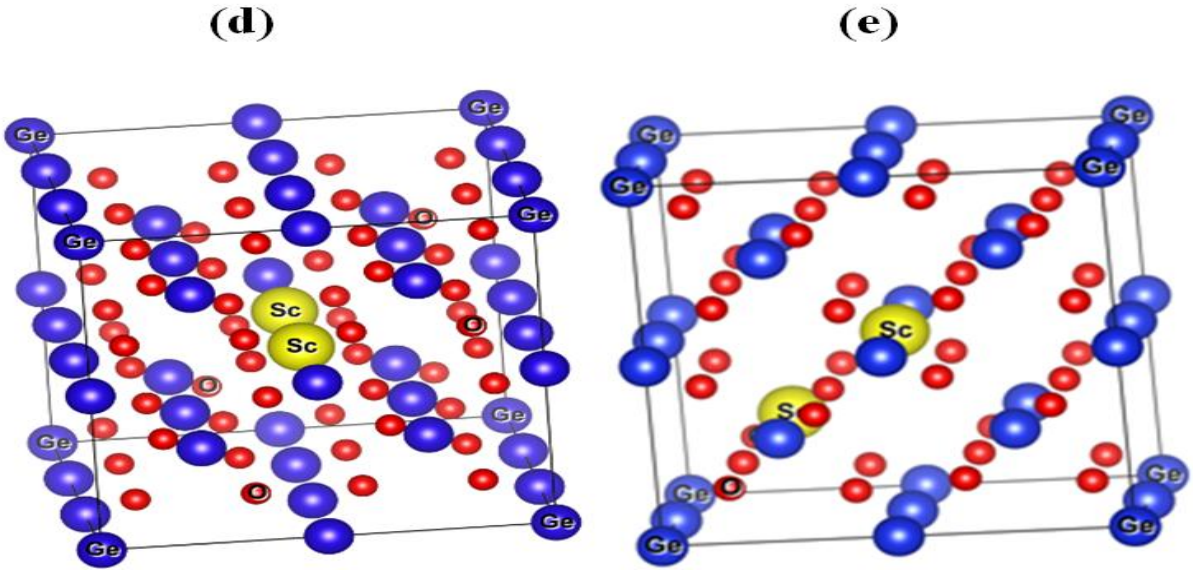


Fig.1. Crystal unit cell of $Sc_xGe_{1-x}O_2$: (a) Un doped r-GeO_2, (b) $Sc_{0,0416}Ge_{0,9584}O_2$,(c) $Sc_{0,0625}Ge_{0,9375}O_2$,(d) $Sc_{0,0833}Ge_{0,917}O_2$, and (e) $Sc_{0,125}Ge_{0,875}O_2$

The effect of Scandium doping on structural and optoelectronic properties of r-GeO_2 was investigated by using two periodic supercells of sizes 2×2×2 and 2×2×3, in which scandium atoms replaced germanium atoms. These supercells contain 48 atoms (16 Ge and 32 O) and 72 atoms (24 Ge and 48 O), respectively.

We considered four doping levels, corresponding to the following concentrations: 4.16%, 6.25%, 8.32%, and 12.5%, associated with the chemical configurations $Sc_{0,0416}Ge_{0,9584}O_2$, $Sc_{0,0625}Ge_{0,9375}O_2$, $Sc_{0,0833}Ge_{0,917}O_2$, and $Sc_{0,125}Ge_{0,875}O_2$ (Fig. 1 b–e).

Doping at 4.16% and 8.32% was achieved by replacing one and two Ge atoms, respectively, with Sc atoms in the 2×2×3 supercell. In comparison, 6.25% and 12.5% doping levels were obtained by replacing one and two Ge atoms with Sc atoms in the 2×2×2 supercell. The criteria for selecting scandium as a dopant are presented in the first section.

The structural parameters of $Sc_xGe_{1-x}O_2$ compounds were obtained by minimizing the total energy, which was calculated by using the GGA-PBE approximation, in accordance with the Murnaghan equation : [55]

$$E(V) = E_0 + \left[\frac{B_0 V}{B'(B'-1)}\right].\left[B'\left(1-\frac{V_0}{V}\right) + \left(\frac{V_0}{V}\right)^{B'} - 1\right] \qquad (1)$$

E_0, V_0, B_0, and B_0' are respectively the energy, volume, compressibility modulus, and its derivative.

The structural optimization results of r- GeO_2 are summarized in Table 1, and compared alongside available theoretical and experimental data . We observe a good agreement with the experimental data. Furthermore, it appears that the GGA approximation has a tendency to

underestimate the lattice constants slightly. In addition, we note that so far, no theoretical study has been performed to compare doped structural properties.

Table 1: The computed structural parametres of Sc-doped r-GeO_2

Compounds	a_0(Å)	c (Å)	u	V_0 (Å)^3	B(GPa)	B'	E_{Tot} (eV)	E_{Form}(eV/atom)
r-GeO_2 pur	4.398*, 4.395[a] 4.45[b],4.477[c] 4.389[d]	2.863* 2.86[a],2.92[b] 2.907[c],2.874[d]	0.305* 0.306[c] 0.307[d]	55.379* 58.28[c]	229.452*	5.351*	-122430.686	- 4.884*
Sc:GeO_2(x=4.16%)	4.405*	2.872*	0.343*	55.729*	224.903*	5.247*	-1432846.266	- 4.911*
Sc:GeO_2(x=6.25%)	4.411*	2.873*	0.347*	55.871*	221.599*	5.136*	-943123.849	- 4.935*
Sc:GeO_2(x=8.32%)	4.416*	2.883*	0.342*	56.163*	216.685*	5.116*	-1396525.065	- 4.948*
Sc:GeO_2(x=12.5%)	4.423*	2.891*	0.347*	56.502*	211.256*	5.098*	-906802.361	- 4.983*

*Present calculations, [a]Ref [10], [b]Ref [53], [c]Ref [54], [d]Ref [28].

We observed an increase in the a and c lattice constants for scandium-doped r-GeO_2 compared to the experimental values of undoped GeO_2 with 1.05%, 1.61%, 2.12%, and 2.82%, corresponding to dopant concentrations of 4.16%, 6.25%, 8.32%, and 12.5%, respectively. (see Fig. 2.a). This is related to the differences in ionic radii between the dopant and the germanium atom; the ionic radius of Ge^{4+} is R (Ge^{4+}) = 0.53 Å [56], while that of Sc^{3+} is R (Sc^{3+}) = 0.745 Å [57]. The substitution of Ge with Sc, therefore, causes a lattice expansion proportional to the concentration of Sc^{3+} introduced.

To investigate the relative stability of scandium-doped r-GeO_2 systems, we computed their formation energies utilizing the following relations [58]

$$\Delta E_{\mathrm{Coh}}(\mathrm{GeO_2\ pure}) = E_{\mathrm{tot}}(\mathrm{GeO_2}) - [2\mathrm{E_{tot}(Ge)} + 4\mathrm{E_{tot}(O)}]/6 \quad (2)$$

$$\Delta E_{\mathrm{Coh}}(\mathrm{Ge_{0.9584}\,Sc_{0.0416}O_2}) = \mathrm{E_{tot}(Ge_{0.9584}\,Sc_{0.0416}O_2)} - [23\ \mathrm{E_{tot}(Ge)} + \mathrm{E_{tot}(Sc)} + 48\ \mathrm{E_{tot}(O)}]/72 \quad (3)$$

$$\Delta E_{\mathrm{Coh}}(\mathrm{Ge_{0.9375}\,Sc_{0.0625}O_2}) = \mathrm{E_{tot}(Ge_{0.9375}\,Sc_{0.0625}O_2)} - [15\ \mathrm{E_{tot}(Ge)} + \mathrm{E_{tot}(Sc)} + 32\ \mathrm{E_{tot}(O)}]/48 \quad (4)$$

$$\Delta E_{\mathrm{Coh}}(\mathrm{Ge_{0.9167}Sc_{0.0833}O_2}) = \mathrm{E_{tot}(Ge_{0.917}Sc_{0.0833}O_2)} - [22\ \mathrm{E_{tot}(Ge)} + 2\mathrm{E_{tot}(Sc)} + 48\ \mathrm{E_{tot}(O)}]/72 \quad (5)$$

$$\Delta E_{\mathrm{Coh}}(\mathrm{Ge_{0.875}Sc_{0.125}O_2}) = \mathrm{E_{tot}(Ge_{0.875}Sc_{0.125}O_2)} - [14\ \mathrm{E_{tot}(Ge)} + 2\mathrm{E_{tot}(Sc)} + 32\ \mathrm{E_{tot}(O)}]/48 \quad (6)$$

E_{tot} (GeO_2), Etot ($Ge_{0.9584}Sc_{0.0416}O_2$), E_{tot} ($Ge_{0.9375}Sc_{0.0625}O_2$), E_{tot} ($Ge_{0.917}Sc_{0.0833}O_2$), and E_{tot} ($Ge_{0.875}Sc_{0.125}O_2$) refer to the total energy of $Ge_{1-x}Sc_xO_2$ compounds with x = 0%, 4.16%, 6.25%, 8.33%, and 12.5%, respectively. At the same time, Etot (Ge), Etot (Sc), and Etot (O) correspond to the total energies of the pure constituent elements (Ge, Sc, and O).

The formation energy values, E_f, calculated for all the compounds studied, are listed in Table 2. For r-GeO_2 doped with 4.16%, 6.25%, 8.33%, and 12.5% Sc, the formation energies are -4.911 eV, -4.935 eV, -4.948 eV, and -4.983 eV, respectively (Fig. 2.b). The negative values confirm the thermodynamic stability of these structures and suggest their feasibility for experimental synthesis.

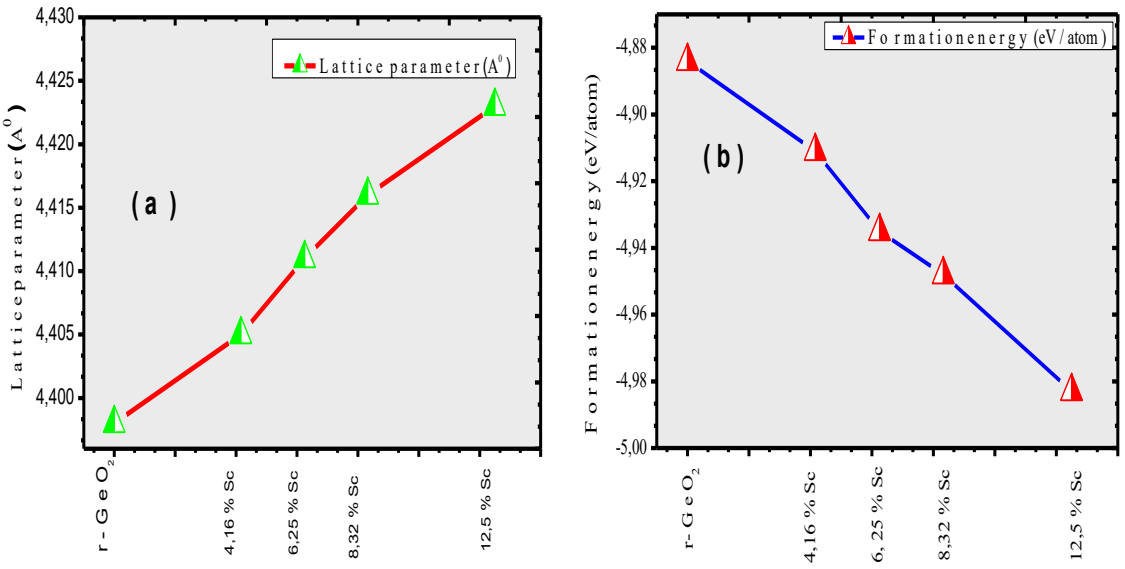


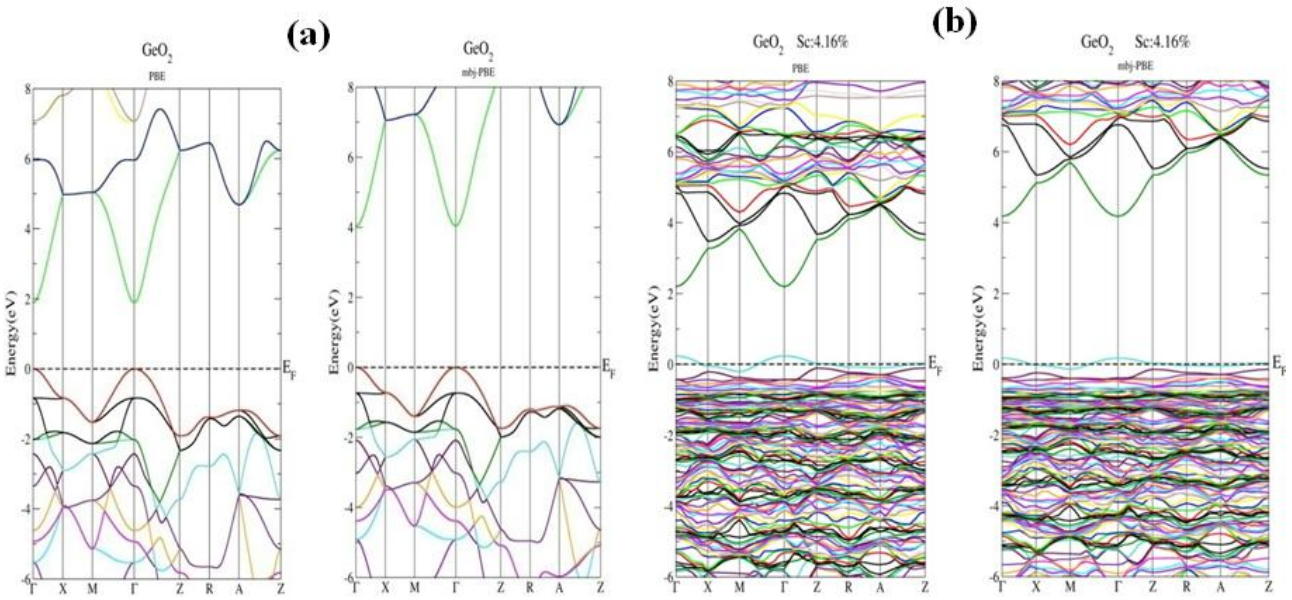
Fig. 2. Lattice parameter and formation energy (ΔH_{form}) variation due to Sc doping in $Sc_xGe_{1-x}O_2$.

In addition, a decrease in the formation energy is observed when the atom of germanium is substituted by an atom of Sc, suggesting that stability of the compounds depends on their anion size. and the thermodynamic stability is generally correlated with the formation energy: However, it is important to note that the experimental synthesis conditions can also influence the value of the formation energy.

Electronic characteristics

Band structure

The band structures of pure (r-GeO_2) and Sc-doped (r-GeO_2) with x = 4.16%, 6.25%, 8.32%, and 12.5%, calculated using mBJ-GGA are shown in Figures 3 (a-e), where the Fermi level (EF) was set as the energy reference at 0 eV and is represented by a dotted line.



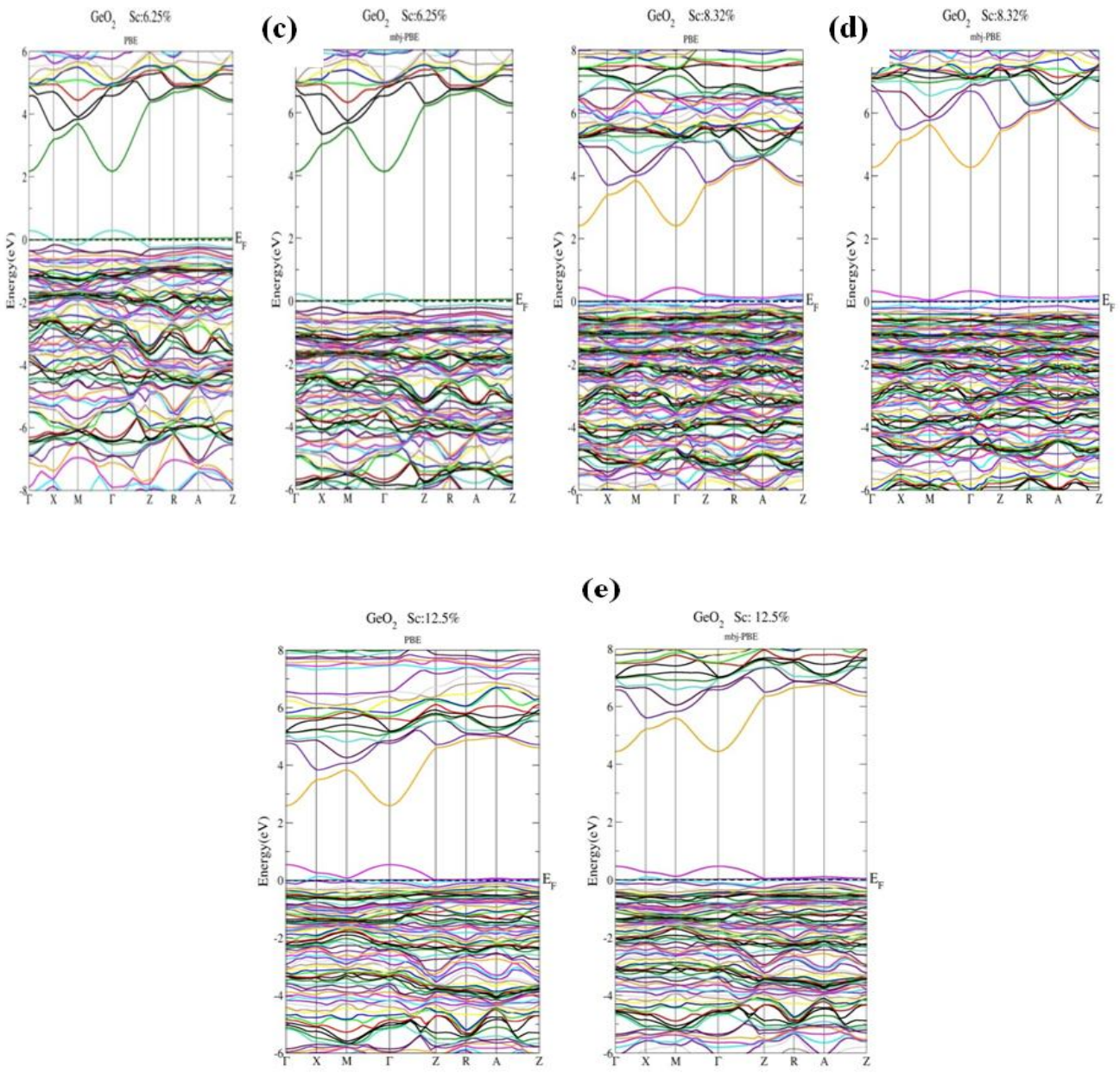


Fig. 3. GGA and TB-mBJ calculated band structure of : (a) pure r-GeO_2, (b) $Sc_{0,0416}Ge_{0,9584}O_2$,(c) $Sc_{0,0625}Ge_{0,9375}O_2$,(d) $Sc_{0,0833}Ge_{0,917}O_2$, and (e) $Sc_{0,125}Ge_{0,875}O_2$

.

The bandgap width for pure r-GeO_2 by GGA-PBE+TB-mBJ is 4.112 eV. This value is slightly higher than the previous result obtained by FP-LAPW (1.80 eV [55]) and lower than some estimates calculated using LDA (2.4 eV [59], 3.12 eV [60]) as well as experimental measures [61]. This discrepancy with experimental data is attributable to the intrinsic limitations of DFT. The energy gap values Eg (eV) for all the studied $Sc_xGe_{1-x}O_2$ materials (x = 0, 4.16%, 6.25%,8.32%, and 12.5%) are shown in Table 2.

Table 2: Bands gaps of $Sc_xGe_{1-x}O_2$ (x = 0, 0.0625, 0.0832 and 0.125) with GGA and TB- mbj

	Present work			
	GGA-PBE	GGA+TB mBJ	Other calculations	Experiments
Pure (r-GeO_2)	1.922*	4.112*	1.80[a], 2.40[b], 3.12[c], 1.25[e], 1.91[f], 4.09[g], 4.10[f], 4.64[h], 4.44[i]	4.68[d]
$Ge_{0.958}Sc_{0.0416}O_2$	1.904*	4.011*	-	-
$Ge_{0.937}Sc_{0.0625}O_2$	1.867*	3.935*	-	-
$Ge_{0.917}Sc_{0.0833}O_2$	1.835*	3.856*	-	-
$Ge_{0.875}Sc_{0.125}O_2$	1.792*	3.778*	-	-

*Present calculations, [a]Ref [28] DFT GGA, [b]Ref [58] DFT-LDA, [c]Ref [59] DFT-LDA, [d]Ref [60] Experiment (UV-absorption),[e]Ref [54] DFT- GGA, [f]Ref [61] DFT- GGA+ mbj, [g]Ref [53] DFT-GGA + mbj, [h]Ref [18] DFT-PAW + HSE06, [i]Ref [4] DFT-LDA + G_0W_0.

The values energy gap of $Sc_xGe_{1-x}O_2$ compounds are 4.011 eV, 3.935 eV, 3.856 eV, and 3.778 eV, corresponding to x = 4.16%, 6.25%, 8.32%, and 12.5%, respectively, as shown in Figures 3 (b-e) noted that Scandium doping results in a narrowing of the bandgap as the concentration of doping increases, by -97.54%, -95.69%, -93.77%, and -91.87% for x = 0.0416, 0.0625, 0.0832, and 0.125, respectively.

This narrowing of the band gap can be attributed to the 3d electrons of the Sc dopant that ease the transfer of electrons from the valence to the conduction bands. As the Fermi level moves to the valence band, this phenomenon is primarily attributable to the characteristics of p-type doping.
We also notice an additional energy barrier arising from the excitation of electrons from their valence to the minimum conduction band states.

The Burstein–Moss effect [62] can explain this observation, which occurs when Sc^{3+} ions substitute for Ge^{4+} ions in the GeO_2 crystal lattice. The adjustment of the Fermi level also contributes to improved electrical conductivity in GeO_2 by facilitating the mobility of charge carriers, which are predominantly p-type.The impurity energy levels (IELs) can act as trapping or recombination centres, as they facilitate electron transitions. So the doping with Sc brings out changes in the electronics and conductivity properties of GeO_2; it opens up possibilities for the use of these doped materials in various electronic and optoelectronic applications.

Density of states

The TDOS and PDOS of pure and Sc-doped r-GeO_2, at x = 4.16%, x = 6.25%, x = 8,32%, and x = 12.5% concentrations were calculated by the GGA+mBJ method, calculated by the mbj-GGA method between -10 and 10 eV, and are given in Figures 4(a – e). The figure 4a illustrate that the valence band (-10 eV -0 eV) of pure GeO_2 is mainly formed by O-2p states, and a slight contributions of Ge-4s and 4p orbitals, In contrast, the conduction band (CB) results from weak hybridization of Ge- 4s and 4p orbitals with 2 p -O . .the absorption edge in the ultraviolet is difined by the electrons moving from O-2p states to Ge-4s states.

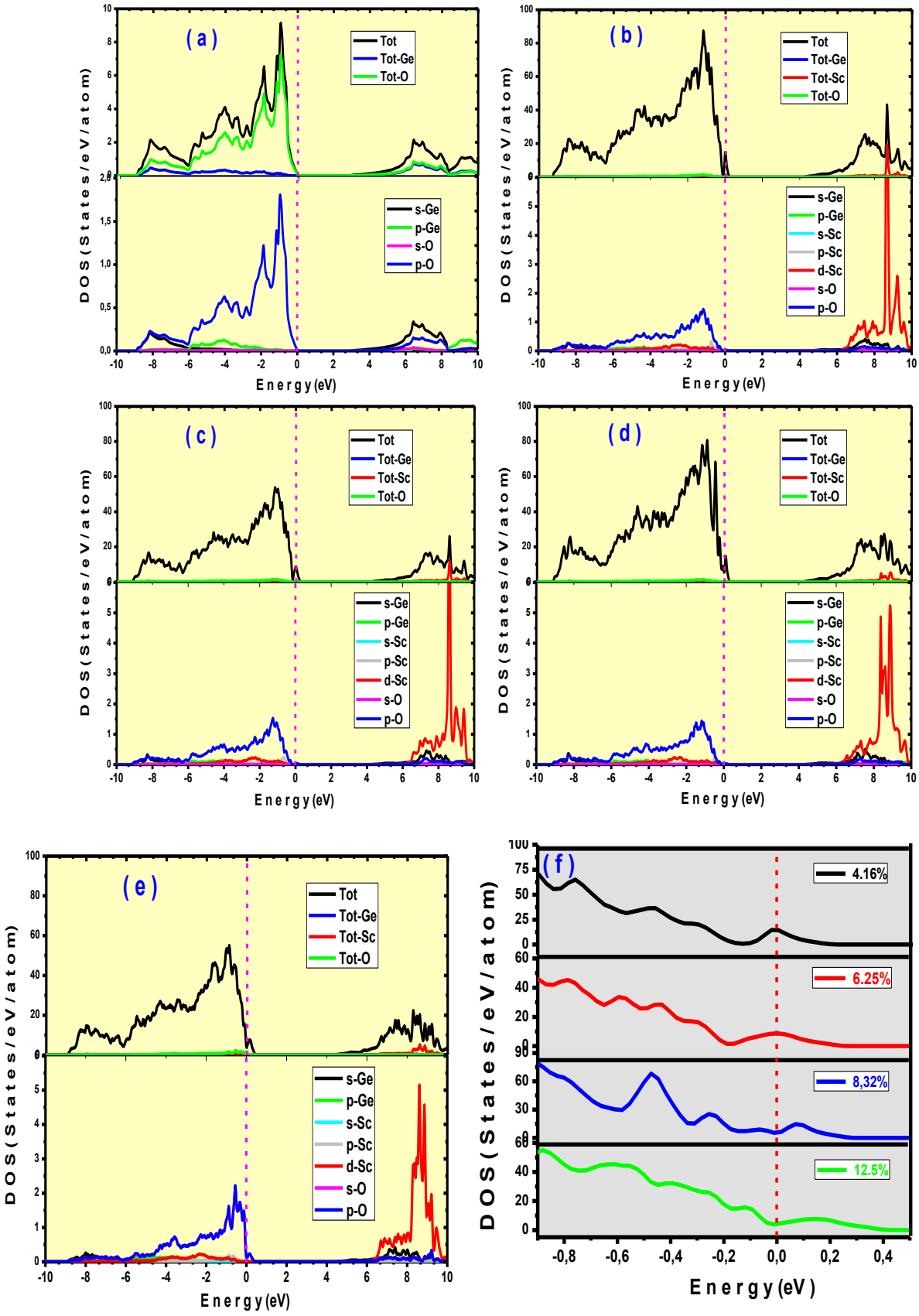


Fig. 4. TB-mBJ calculated TDOS and PDOS of $Sc_xGe_{1-x}O_2$: (a) x = 0, (b) x = 4.16%,(c) x = 6.25%,(d) x = 8.32%, (e) x = 12.5% and (f) compared TDOS of syetems doped.

Figures 4(b – e) presents the TDOS and PDOS of $Sc_xGe_{1-x}O_2$ (x = 4.16%, 6.25%, and 12.5%). The TDOS reveals a behaviour typical of semiconductors in each of these compounds, where the Sc-3d orbitals are responsible for an intense peak located between 6.35 eV and 10 eV, indicating a significant contribution from localized states in this region of the conduction band. Furthermore, marked hybridization between the p states of oxygen and the d states of Sc is observed in the valence band. This hybridization is crucial in the formation of the valence and conduction states, thereby influencing the bandgap width and the conductivity of the compounds. The bandgap values are consistent with the calculated band structures, showing a decrease in the bandgap as the Sc concentration increases. This reduction is due to the contribution of O-2p states in the VB and Sc-3d states in the CB, compared to pure GeO_2 . It is observed that the TDOS values for pure GeO_2 and Sc-doped GeO_2 are respectively 87.12 eV and 53.831 eV, due to the number of outer valence electrons in Ge, Sc, and O atoms.

The Sc-doping creates extra carriers in the VBM, close to Fermi energy of GeO_2. This is because the Sc atom has fewer outer valence electrons than the Ge atom, resulting in p-type doping. As shown in Figure 4.f, the fact that the scandium concentration increases near the Fermi level helps reduce the number of occupied states, as demonstrated by Slassi et al. [63]. The significant contribution of O-2p states at the top of the valence band (VBM) in oxide-based semiconductors leads to a decrease in p-type conductivity.

Results of optical properties

To evaluate the impact of intermediate bands (IB) on optical properties, we analyzed the dielectric function of pure r-GeO_2 and Sc-doped compounds (x = 4.16%, 6.25%, 8.32%, and 12.5%), as this parameter allows for all optical properties to be determined and can be expressed [64]:

$$\varepsilon(\omega) = \varepsilon_1(\omega) + i\varepsilon_2(\omega) \quad (7)$$

$\varepsilon_1(\omega)$ and $\varepsilon_2(\omega)$ are given by the Kramers-Kronig relations [65, 66]:

$$\varepsilon_1(\omega) = 1 + \frac{2}{\pi} P \int_0^{\infty} \frac{\varepsilon_2(\omega')\omega' d\omega'}{\omega'^2 - \omega^2} \quad (8)$$

$$\varepsilon_2(\omega) = \frac{8}{3\pi\omega^2} \sum_{n\dot{n}} \int |P_{n\dot{n}}(k)|^2 \frac{dS_k}{\nabla\omega_{n\dot{n}}(k)} \quad (9)$$

Figures 5. a and b illustrates the variation of the components $\varepsilon_1(\omega)$ and $\varepsilon_2(\omega)$ as a photon energy from 0 eV up to 5 eV for all compounds studied.An optical anisotropy is observed in the infrared spectral range for all of the compounds. The ε_1 component of $Ge_{0.917}Sc_{0.0832}O_2$ and $Ge_{0.875}Sc_{0.125}O_2$ is decreased and cancelled around 0.42 eV and 0.25 eV, respectively (Fig. 5.a). The static dielectric constant $\varepsilon_1(0)$ is dominated by a real part $\varepsilon_1(\omega)$ and refractive index at the measurement frequency, higher than the frequencies of lattice vibrations in these crystals [67].

The static dielectric permittivity values at low energy are 2.16 for pure r-GeO_2, while those of GeO_2 doped with Sc are 5.99, 6.92, 20.21, and 36.16 for x = 4.16%, 6.25%, 8.32%, and 12.5%, respectively(Table 3). This suggests that the introduction of scandium into doped compounds

increases the static dielectric constant. And a narrowing of the forbidden energy band. This observation is explained according to Penn's model [68] :

$$\varepsilon_1(0) \simeq 1 + \left(\frac{\omega_p}{E_g}\right)^2 \qquad (10)$$

ω_p and E_g are the plasma frequency and energy band gap respectively.

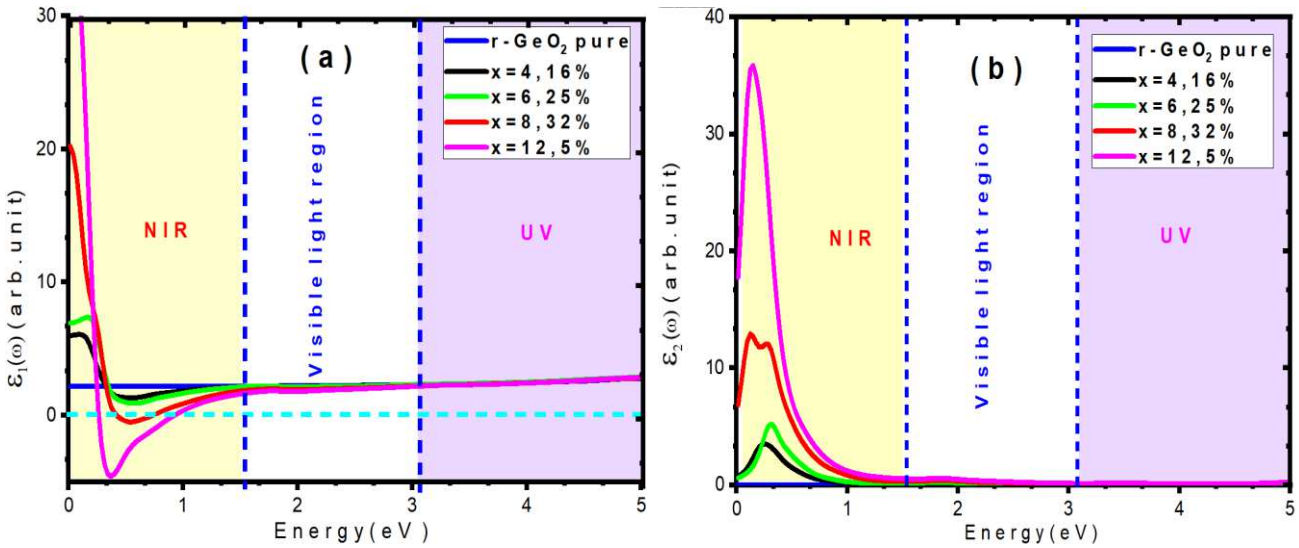


Fig. 5. Dielectric function of pure and Sc-doped r-GeO_2 : (a) real part ε_1 and (b) imaginary part ε_2

For pure r-GeO_2, the observed $\varepsilon_2(\omega)$ values stayed at zero. This means that no absorption has been noted because the photo energy was insufficient to induce electronic excitations. The imaginary spectra of dielectric function show an intense peak at low energies, with maximum values at 0.23 eV, 0.31 eV, 0.12 eV, and 0.15 eV for $Ge_{0.9584}Sc_{0.0416}O_2$, $Ge_{0.9875}Sc_{0.0625}O_2$, $Ge_{0.918}Sc_{0.0882}O_2$ and $Ge_{0.875}Sc_{0.125}O_2$, respectively. A comparative analysis of pure and doped r-GeO_2 spectra demonstrates that Sc doping results in an increase of absorption in the IR region (Fig. 5.b). The calculated of $\varepsilon_1(\omega)$ and $\varepsilon_2(\omega)$ should be used to determine other optical properties, such as absorption coefficient $\alpha(\omega)$, reflectivity $R(\omega)$, optical conductivity $\sigma(\omega)$, refractive index $n(\omega)$, extinction coefficient $k(\omega)$, and energy loss $L(\omega)$ [69] according to equations (11) through (16).

$$\alpha(\omega) = \frac{4\pi}{\lambda} k(\omega) \qquad (11)$$

$$R(\omega) = \frac{(n-1)^2+K^2}{(n+1)^2+K^2} \qquad (12)$$

$$\sigma(\omega) = \sigma_1(\omega) + i\sigma_2(\omega) = -i\,\frac{\omega}{4\pi}[\varepsilon(\omega) - 1] \qquad (13)$$

$$n(\omega) = \frac{1}{\sqrt{2}}\left[(\varepsilon_1{}^2(\omega) + \varepsilon_2{}^2(\omega))^{\frac{1}{2}} + \varepsilon_1(\omega)\right]^{\frac{1}{2}} \qquad (14)$$

$$K(\omega) = \frac{1}{\sqrt{2}}\left[(\varepsilon_1{}^2(\omega) + \varepsilon_2{}^2(\omega))^{\frac{1}{2}} - \varepsilon_1(\omega)\right]^{\frac{1}{2}} \qquad (15)$$

$$L(\omega) = Im\left(\frac{-i}{\varepsilon(\omega)}\right) = \frac{\varepsilon_2(\omega)}{\varepsilon_1{}^2(\omega)+\varepsilon_2{}^2(\omega)} \qquad (16)$$

Figure 6.a. shows the absorption spectrum of $Sc_xGe_{1-x}O_2$ compounds (x = 0, 4.16%, 6.25%, 8.32%, and 12.5%).The undoped r-GeO_2 exhibits a strong absorption in the ultraviolet region corresponding to the energy gap between O-2p and Ge-4p electron energy levels.

The appearance of these transitions suggests the influence of oxygen vacancies on the optical properties of GeO_2, which leads to an extended absorption from visible to ultraviolet spectra.

The absorption peaks for the doped compounds $Ge_{0.9584}Sc_{0.0416}O_2$, $Ge_{0.9875}Sc_{0.0625}O_2$, $Ge_{0.918}Sc_{0.0882}O_2$ and $Ge_{0.875}Sc_{0.125}O_2$ are concentrated in the UV region, suggesting high absorption in this range. These observations show that there are significant electronic transitions induced by Sc^{3+} ions, and localized electronic orbitals associated with Ge-Sc interactions.

The $Sc_xGe_{1-x}O_2$ compounds (x = 0, 4.16%, 6.25%, 8.32%, and 12.5%) exhibit new absorption peaks in the visible region (400–800 nm), with an absorption coefficient α located approximately at 1.86 eV.This absorption is attributable to structural defects or oxygen vacancies exacerbated by doping. In addition, an increase in Sc concentration induces a shift of the absorption threshold toward longer wavelengths, leading to a gradual reduction in the bandgap width. These results underscore the significant influence of the Sc dopant on the optical properties of rutile GeO_2, and show that the strength of the induced transitions as well as the shift in the absorption threshold are proportional to the dopant concentration. As a result, these doped materials offer significant flexibility for the development of advanced components in optoelectronic technologies.

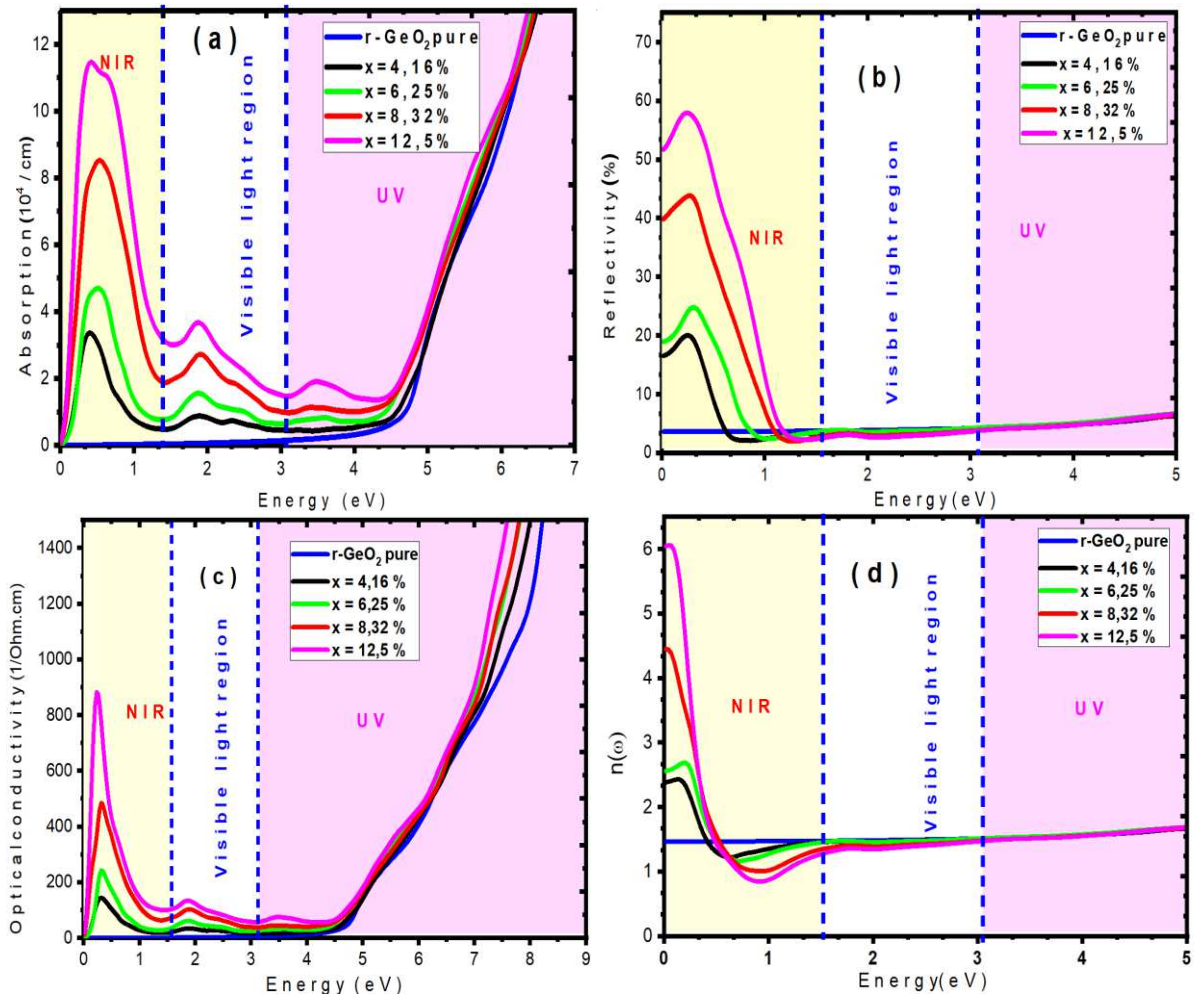


Fig. 6. Comparison of : (a) absorption α(ω), (b) reflectivity R(ω), (c) conductivity σ(ω) and (d) refractive index of pure and Sc-doped r-GeO_2 systems.

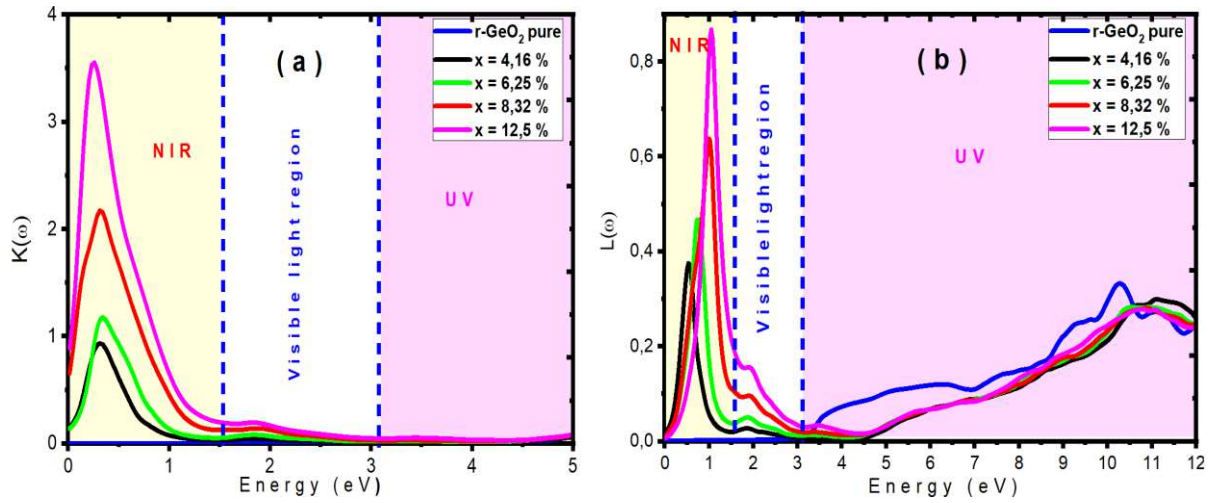


Fig. 7. Extinction index k(ω) (a) and loss function L(ω) (b) of pure and Sc-doped r-GeO_2 systems.

Figure 6.b also shows the reflectivity spectra R(ω) as a function of energy for pure r-GeO_2, $Ge_{0.9584}Sc_{0.0416}O_2$, $Ge_{0.9875}Sc_{0.0625}O_2$, $Ge_{0.918}Sc_{0.0882}O_2$ and $Ge_{0.875}Sc_{0.125}O_2$. The most intense reflectivity peaks are observed in the infrared region, with respective maximum values of approximately 20.06%, 24.74%, 43.87%, and 57.96%. Consequently, these materials exhibit very low reflectivity in the visible and ultraviolet ranges.

The R(0) values are 3.62%, 16.57%, 18.96%, 39.86%, and 51.72%, corresponding to concentrations x = 0, 0.0416, 0.0625, 0.0832, and 0.125 (Table 3).It is observed that their reflectivity increases with increasing Sc concentration, which means that doping with Sc^{3+} effectively increases the reflectivity of pure r-GeO_2.

The optical conductivity σ(ω of doped and undoped systems is shown in Figure 6.c. We observed that for doped r-GeO_2, the optical conductivity σ(ω) reaches its maximum values in the infrared region, around 144.86 $(ohm\cdot cm)^{-1}$, 242.71 $(ohm\cdot cm)^{-1}$, 484.61 $(ohm\cdot cm)^{-1}$ and 882.91 $(ohm\cdot cm)^{-1}$, which correspond to concentrations of x = 4.16%, 6.25%, 8.32%, and 12.5%, respectively. This can be explained by the electronic transitions from the CBM to the VBM via the intermediate states introduced by the Sc^{3+} impurity; thus, the latter acts as a modifier of the electronic structure and conductivity of r-GeO_2 rutile. The optical conductivity then decreases gradually up to the visible light spectrum. It is clear that both pure and doped GeO_2 compounds in the ultraviolet range present very high optical conductivity, which indicates their usefulness in many modern optoelectronic devices.

The calculated of refractive index n (ω) is depicted in Figure 6.d. At zero frequency, the static value n (0) obtained for pure r-GeO_2, without an exciton peak, is 1.46. The refractive index then increases with scandium doping, reaching 2.38, 2.56, 4.45, and 6.04 for $Ge_{0.9584}Sc_{0.0416}O_2$, $Ge_{0.9875}Sc_{0.0625}O_2$, $Ge_{0.918}Sc_{0.0882}O_2$ and $Ge_{0.875}Sc_{0.125}O_2$ compounds (Table 3).

According to this figure, for doped systems, we observe a decrease in the refractive spectra in range of 1.55 to 3.1 eV, followed by an increase up to the visible part of the spectrum. For $Sc_xGe_{1-x}O_2$ (x = 12.5%), n(ω) decreases to 0.84 (<1), indicating that the group velocity of the incident

radiation can exceed the speed of light [70]. A refractive index variation as small as this for r-GeO_2 means that it is a promising candidate for applications needing a low chromatic dispersion.

Figure 7.a shows the variation of extinction coefficient k(ω) for all compounds studied. A similar trend is observed between the absorption and extinction coefficients due to the intrinsic relation between them (Figure 6.a and 6.d). For energies up to 0.71 eV, ε_2 starts to increase and attains a maximum of 0.93 for $Ge_{0.9584}Sc_{0.0416}O_2$, 1.17 eV for $Ge_{0.9875}Sc_{0.0625}O_2$, 2.18 eV for $Ge_{0.918}Sc_{0.0882}O_2$, and 3.55 eV for $Ge_{0.875}Sc_{0.125}O_2$. Thereafter, it decreases rapidly. Furthermore, these materials exhibit negligible extinction coefficients at low energies. The evolution of the spectrum (E) is entirely consistent with that obtained for the ε_2 (E) spectrum. The static values of k(0) at zero frequency are regrouped in Table 3.

Table 3: The evaluated of optical constants for $Sc_xGe_{1-x}O_2$ (x = 0, 0.0625, 0.0832 and 0.125)

Compounds	$\varepsilon_1(0)$	R(0) %	n(0)	k(0)
r-GeO_2 pur	2.16	3,62	0	0
Sc:GeO_2(x=4.16%)	5.99	16.57	2,38	0.15
Sc:GeO_2(x=6.25%)	6.92	18,96	2.56	0.14
Sc:GeO_2(x=8.32%)	20.21	39,86	4,45	0.65
Sc:GeO_2(x=12.5%)	36.16	51,72	6,04	0.88

Figure 7.b shows the L(ω) curves of calculated compounds between 0 and 12 eV. In the IR region, the main peaks of the $Sc_xGe_{1-x}O_2$ compounds (x = 0, 4.16%, 6.25%, 8.32%, and 12.5%) appear at 0.53 eV, 0.63 eV, and 0.66 eV, respectively. This indicates that doping GeO_2 with Sc causes a shift of the main peaks toward higher energies (ultraviolet shift) and that the intensity of these peaks increases with increasing Sc content.

L(ω) has a minimum in the visible region, whereas above ~3 eV, all spectra show a gradual increase, corresponding to volume plasmon excitations or interband transitions typical of GeO_2. These observations confirm that the study of energy loss spectra is a powerful tool for analysis of the effect of doping on the plasmonic and electronic characteristics of solids.

Conclusion

In conclusion, we have investigated the structural, electronic, and optical properties of r-GeO_2 by incorporating Scandium at contents ranging from 4.16% to 12.5%, using first-principles calculations. Ab-initio methods, within the framework of density functional theory and the modified Becke–Johnson potential, were employed in this study. Structural analysis reveals that the lattice parameter increases as Sc replaces Ge, and the compressibility modulus decreases with increasing Sc content. Our compounds are thermodynamically stable, as evidenced by their negative formation energies. Due to their stability, these systems are likely to exist in nature.

Electronic band structure calculations indicate that these systems exhibit a direct bandgap (Γ-Γ), with the introduction of Sc into the r-GeO_2 matrix effectively reducing the bandgap. The Fermi level shifts toward the bottom of the valence band, suggesting the properties of a p-type material. According to the density of states (DOS) analysis, the 3d orbitals of Sc show occupied states near the

Fermi level, which play a crucial role in enhancing the optoelectronic characteristics of these materials.

The optical characteristics exhibited marked anisotropy due to their absorption and maximum optical conductivity, which are estimated to occur at high energies. This finding highlights the potential of Scandium as a promising dopant for enhancing the UV-sensitive optoelectronic response of GeO_2-based devices. Future work should focus on the experimental verification of the predicted modification of the bandgap and optical absorption, in order to validate the theoretical conclusions and guide the development of advanced optoelectronic devices for UV detection.

Acknowledgments

We would like to thank Professor Chercheb of Laboratory of Micro and Nanophysics (LaMiN) National Polytechnic School Oran, ENPO-MA for her support during of this study.

Statements and Declarations

The authors declare that they have no known competing personal relationships or financial interests that could appear to influence the work reported in this paper.

Funding Declaration

This research received no external funding

References

[1] Tsao JY, Chowdhury S, Hollis MA, Jena D, Johnson NM, Jones KA, Kaplar RJ, Rajan S, Van de Walle CG, Bellotti E, Chua CL, Collazo R, Coltrin ME, Cooper JA, Evans KR, Graham S, Grotjohn TA, Heller ER, Higashiwaki M, Islam MS, Juodawlkis PW, Khan MA, Koehler AD, Leach JH, Mishra UK, Nemanich RJ, Pilawa-Podgurski RCN, Shealy JB, Sitar Z, Tadjer MJ, Witulski AF, Wraback M, Simmons JA (2018) Ultrawide-bandgap semiconductors: research opportunities and challenges. Adv Electron Mater 4:1600501. doi.org/10.1002/aelm.201600501

[2] Kim S, Moon J, Bae S, Xu Z, Meng Y, Park J, Lee J, Bae S (2025) Freestanding wide-bandgap semiconductors nanomembrane from 2D to 3D materials and their applications. Small Methods 9:2401551. doi.org/10.1002/smtd.202401551

[3] Qin Y, Albano B, Spencer J, Lundh JS, Wang B, Buttay C, Tadjer M, DiMarino C, Zhang Y (2023) Thermal management and packaging of wide and ultra-wide bandgap power devices: a review and perspective. J Phys D Appl Phys 56:093001. doi.org/10.1088/1361-6463/acb4ff

[4] Chae S, Mengle K, Bushick K, Lee J, Sanders N, Deng Z, Mi Z, Poudeu PFP, Paik H, Heron JT, Kioupakis E (2021) Toward the predictive discovery of ambipolarly dopable ultra-wide-band-gap semiconductors: The case of rutile GeO_2. Appl Phys Lett 118:262101. doi.org/10.1063/5.0056674

[5] Sierra JH, Carvalho DO, Kassab LR, da Silva Bordon CD, Samad RE, Wetter NU, Alayo MI (2021) Pedestal waveguides based on GeO_2-Bi_2O_3, GeO_2-PbO, Ta_2O_5 and SiO_xN_γ cores as platforms for optical amplifiers, and nonlinear optics applications: Review of recent advances. J Lumin 236:118113. doi.org/10.1016/j.jlumin.2021.118113

[6] Grimsditch M, Polian A, Brazhkin V, Balitskii D (1998) Elastic constants of α-GeO_2. J Appl Phys 83:3018–3020. doi.org/10.1063/1.367117

[7] Suzuki T, Sakaban K, Katase T, Yoshida H, Hiramatsu H, Hosono H, Kamiya T (2025) Phase diagram and growth mechanism of rutile-type GeO_2 epitaxial film on c-plane sapphire substrate. ACS Appl Nano Mater 8:7796–7805. doi.org/10.1021/acsanm.5c01137
[8] Nagashima Y, Osawa S, Oka D, Hirose Y (2025) Solid phase epitaxy of rutile-type GeO_2 on TiO_2 (001). Appl Phys Lett 127:172103. doi.org/10.1063/5.0271675
[9] Walker B, Dharmawardhana CC, Dari N, Rulis P, Ching WY (2015) Electronic structure and optical properties of amorphous GeO_2 in comparison to amorphous SiO_2. J Non-Cryst Solids 428:176–183. doi.org/10.1016/j.jnoncrysol.2015.08.018
[10] Bolzan AA, Fong C, Kennedy BJ, Howard CJ (1997) Structural studies of rutile-type metal dioxides. Acta Cryst B 53:373–380. doi.org/10.1107/S0108768197001468
[11] Micoulaut M, Cormier L, Henderson GS (2006) The structure of amorphous, crystalline and liquid GeO_2. J Phys Condens Matter 18. doi.org/10.1088/0953-8984/18/45/R01
[12] Bielz T, Soisuwan S, Girgsdies F, Klötzer B, Penner S (2012) Reduction of different GeO_2 polymorphs. J Phys Chem C 116:9961–9968. doi.org/10.1021/jp2123456
[13] Liu QJ, Liu ZT (2014) Structural, elastic, and mechanical properties of germanium dioxide from first-principles calculations. Mater Sci Semicond Process 27:765–771. doi.org/10.1016/j.mssp.2014.07.047
[14] Shieh SR, Kubo A, Duffy TS, Prakapenka VB, Shen G (2006) High-pressure phases in SnO_2 to 117 GPa. Phys Rev B 73:014105. doi.org/10.1103/PhysRevB.73.014105
[15] Haines J, Léger JM (1997) X-ray diffraction study of the phase transitions and structural evolution of tin dioxide at high pressure: relationships between structure types and implications for other rutile type dioxides. Phys Rev B 55:11144–11152. doi.org/10.1103/PhysRevB.55.11144
[16] Bayerl D, Kioupakis E (2015) Theoretical limits of thermoelectric figure of merit in n-type TiO_2 polymorphs. Phys Rev B 91:165104. doi.org/10.1103/PhysRevB.91.165104
[17] Mernagh TP, Liu L-G (1997) Temperature dependence of Raman spectra of the quartz- and rutile-types of GeO_2. Phys Chem Miner 24:7–16. doi.org/10.1007/s002690050012
[18] Chae S, Lee J, Mengle KA, Heron JT, Kioupakis E (2019) Rutile GeO_2: an ultrawide-bandgap semiconductor with ambipolar doping. Appl Phys Lett 114:101903. doi.org/10.1063/1.5088370
[19] Mengle KA, Chae S, Kioupakis E (2019) Quasiparticle band structure and optical properties of rutile GeO_2, an ultra-wide-band-gap semiconductor. J Appl Phys 126:085703. doi.org/10.106 3/1.5111318
[20] Labed M, Jeon HJ, Park JH, Pearton SJ, Rim YS (2025) Rutile germanium dioxide: An emerging ultrawide bandgap semiconductor for power device applications – A review. Mater Today 83:513–537. doi.org/10.1016/j.mattod.2025.01.012
[21] Sozen Y, Yagmurcukardes M, Sahin H (2021) Vibrational and optical identification of GeO_2 and GeO single layers: a first-principles study. Phys Chem Chem Phys 23:21307–21315. doi.org/10.1039/D1CP02299G
[22] Bose N, Basu M, Mukherjee S (2012) Study of optical properties of GeO_2 nanocrystals as synthesized by hydrothermal technique. Mater Res Bull 47:1368–1373. doi.org/10.1016/j. materresbull.2012.03.009
[23] Galazka Z, Blukis R, Fiedler A, Anooz SB, Zhang J, Albrecht M, Remmele T, Schulz T, Klimm D, Pietsch M, Kwasniewski A, Dittmar A, Ganschow S, Juda U, Stolze K, Suendermann M,

Schroeder T, Bickermann M (2025) Bulk single crystals and physical properties of rutile GeO_2 for high-power electronics and deep-ultraviolet optoelectronics. Phys Status Solidi B 262:2400326. doi.org/10.1002/pssb.202400326
[24] Hwang M, Chung J, Ryu B, Liyu J (2024) GeO_2-based novel optical glasses with high refractive index, large mid-infrared transmission, and low thermal expansion. J Korean Ceram Soc 61:896–905. doi.org/10.1007/s43207-024-00407-8
[25] Wan W, Peng Y, Ge Y, Fu B, Liu Y (2024) Robust in-plane ferroelectricity, high hole mobility, and low thermal conductivity in GeO monolayer: A first-principles study. Physica E 162:115997. doi.org/10.1016/j.physe.2024.115997
[26] Tetzner K, Galazka Z, Thies A, Külberg A, Hilt O (2026) Lateral rutile GeO_2 MOSFET devices on single-crystal r-GeO_2 substrates. IEEE Electron Device Lett 47:566–569. doi.org/10.1109/LED.2025.3638262
[27] Ravindra RM, Weeks RA, Kinser DL (1987) Optical properties of GeO_2. Phys Rev B 36:6132–6135. doi.org/10.1103/PhysRevB.36.6132
[28] Sahnoun M, Daul C, Khenata R (2005) Optical properties of germanium dioxide in the rutile structure. Eur Phys J B 45:455–458. doi.org/10.1140/epjb/e2005-00219-y
[29] Peng M, Meng X, Qiu J, Zhao Q, Zhu C (2005) GeO_2, M (M = Ga, B) glasses with superwide infrared luminescence. Chem Phys Lett 403:410–414. doi.org/10.1016/j.cplett.2005.01.054
[30] Seal M, Bose N, Mukherjee S (2018) Application of GeO_2 nanoparticles as electrically erasable memory and its photocatalytic behaviour. Mater Res Express 5:065007. doi.org/10.1088/2053-1591/aac66b
[31] Zhang A, Liang Y, Zhang H, Geng Z, Zeng J (2021) Doping regulation in transition metal compounds for electrocatalysis. Chem Soc Rev 50:9817–9844. doi.org/10.1039/D1CS00330E
[32] Yan Y, Wei S-H (2008) Doping asymmetry in wide-bandgap semiconductors: origins and solutions. Phys Status Solidi B 245:641–652. doi.org/10.1002/pssb.200743334
[33] Schleife A, Varley JB, Fuchs F, Rödl C, Bechstedt F, Rinke P, Janotti A, Van de Walle CG (2011) Tin dioxide from first principles: quasiparticle electronic states and optical properties. Phys Rev B 83:035116. doi.org/10.1103/PhysRevB.83.035116
[34] Varley JB, Janotti A, Franchini C, Van de Walle CG (2012) Role of self-trapping in luminescence and n-type conductivity of wide-band-gap oxides. Phys Rev B 85:081109. doi.org/10.1103/PhysRevB.85.081109
[35] Hu W, Peterson RL (2017) The roles of rare-earth dopants in solution-processed ZnO-based transparent conductive oxides. J Appl Phys 122:105301. doi.org/10.1063/1.4991943
[36] Boujnah M, Ennaceri H, Belasfar K, El Kenz A, Benyoussef A, Loulidi M, Ahmed E (2016) New transparent conducting oxide based on doped SnO_2 for solar cells. Inter Renew Sustain Energy (IRSEC):229–233. doi.org/10.1109/IRSEC.2016.7983960
[37] Khan M, Cao W (2013) Chemical preparation of Y-doped TiO_2 by hydrothermal method and investigation of its visible light photocatalytic activity by the degradation of methylene blue. J Mol Catal A Chem 376:71–77. doi.org/10.1016/j.molcata.2013.04.009
[38] Qodziana Z, Parlinski K (2001) Ab initio studies of high-pressure transformations in GeO_2. J Phys Condens Matter 63:134106. doi.org/10.1103/PhysRevB.63.134106

[39] Samanta A, Jain M, Singh AK (2015) Ultra-sensitive pressure dependence of bandgap of rutile-GeO_2 revealed by many body perturbation theory. J Chem Phys 143:064703. doi.org/10.1063/1.4928526
[40] Giacomazzi L, Pasquarello A (2007) Vibrational spectra of vitreous SiO_2 and vitreous GeO_2 from first principles. J Phys Condens Matter 19:415112. doi.org/10.1088/0953-8984/19/41/415112
[41] Kibalchenko M, Yates JR, Pasquarello A (2010) First-principles investigation of the relation between structural and NMR parameters in vitreous GeO_2. J Phys Condens Matter 22:145501. doi.org/10.1088/0953-8984/22/14/145501
[42] Golze D, Iannuzzi M, Hutter J (2017) Local fitting of the Kohn–Sham density in a Gaussian and plane waves scheme for large-scale density functional theory simulations. J Chem Theory Comput 13:2202–2214. doi.org/10.1021/acs.jctc.7b00148
[43] Clark RD (2014) Emerging applications for high-k materials in VLSI technology. Materials 7:2913–2944. doi.org/10.3390/ma7042913
[44] Lu C, Lee CH, Zhang W, Nishimura T, Nagashio K, Toriumi A (2014) Enhancement of thermal stability and water resistance in yttrium-doped GeO_2/Ge gate stack. Appl Phys Lett 104:092909. doi.org/10.1063/1.4868032
[45] Blaha P, Schwarz K, Madsen GKH, Kvasnicka D, Luitz J (2001) WIEN2k, an augmented plane wave plus local orbital program for calculating crystal properties. Vienna University of Technology, Vienna.
[46] Blaha P, Schwarz K, Tran F, Laskowski R, Madsen GKH, Marks LD (2020) WIEN2k: An APW+lo program for calculating the properties of solids. J Chem Phys 152:074101. doi.org/10.1063/1.5143061
[47] Hohenberg P, Kohn W (1964) Inhomogeneous electron gas. Phys Rev 136–B871. doi.org/10.1103/PhysRev.136.B864
[48] Kohn W, Sham LJ (1965) Self-consistent equations including exchange and correlation effects. Phys Rev 140. doi.org/10.1103/PhysRev.140.A1133
[49] Lee IH, Martin RM (1997) Applications of the generalized-gradient approximation to atoms, clusters, and solids. Phys Rev B 56:7197. doi.org/10.1103/PhysRevB.56.7197
[50] Perdew JP, Burke K, Ernzerhof M (1996) Generalized gradient approximation made simple. Phys Rev Lett 77:3865. doi.org/10.1103/PhysRevLett.77.3865
[51] Wang Y, Wisesa P, Balasubramanian A, Dwaraknath S, Mueller T (2021) Rapid generation of optimal generalized Monkhorst-Pack grids. Comput Mater Sci 187:110100. doi.org/10.1016/j.commatsci.2020.110100
[52] Golbasi F, Liu B, Hwang J, Akyol F (2025) Characteristics of single crystalline rutile GeO_2 film grown on sapphire by chemical vapor deposition with a high growth rate ~2.2 μm/hr. J Alloys Compd 1014:178591. doi.org/10.1016/j.jallcom.2025.178591
[53] Ziat Y, Belkhanchi H, Zarhri Z (2025) DFT analysis of structural, electrical, and optical properties of S, Si, and F-doped GeO_2 rutile: Implications for UV-transparent conductors and photodetection. J Sci Eng Solid State 14:1. doi.org/10.51646/jsesd.v14i1.232
[54] Liu QJ, Liu ZT, Feng LP, Tian H (2010) First-principles study of structural, elastic, electronic and optical properties of rutile GeO_2 and α-quartz GeO_2. Solid State Sci 12:1748–1755. doi.org/10.1016/j.solidstatesciences.2010.07.025

[55] Murnaghan FD (1944) The compressibility of media under extreme pressures. Proc Natl Acad Sci USA 30:244–247. doi.org/10.1073/pnas.30.9.244
[56] Cotton SA (1999) The co-ordination number of Sc^{3+}(aq), a journal of critical discussion of the current literature. J Crit Discuss Curr Lit 21:165–173. doi.org/10.1080/02603599908020421
[57] Sun J, Ruzsinszky A, Perdew JP (2015) Strongly constrained and appropriately normed semilocal density functional. Phys Rev Lett 115:036402. doi.org/10.1103/PhysRevLett.115.036402
[58] Christie DM, Chelikowsky JR (2000) Electronic and structural properties of germania polymorphs. Phys Rev B 62:14703–14711. doi.org/10.1103/PhysRevB.62.14703
[59] Sevik C, Bulutay C (2007) Theoretical study of the insulating oxides and nitrides: SiO_2, GeO_2, Al_2O_3, Si_3N_4, and Ge_3N_4. J Mater Sci 42:6555–6565. doi.org/10.1007/s10853-007-1526-9
[60] Stapelbroek M, Evans BD (1978) Exciton structure in the UV-absorption edge of tetragonal GeO_2. Solid State Commun 25:959–962. doi.org/10.1016/0038-1098(78)90311-3
[61] Singh H, Singh M, Kumar S, Kashyap MK (2011) Full potential calculation of electronic properties of rutile RO_2 (R = Si, Ge, Sn, and Pb) compounds via modified Becke-Johnson potential. Physica B 406:3825–3830. doi.org/10.1016/j.physb.2011.07.004
[62] Burstein E (1954) Anomalous optical absorption limit in InSb. Phys Rev 93:632–633. doi.org/10.1103/PhysRev.93.632
[63] Slassi A (2016) Ab initio study on the structural, electronic, optical and electrical properties of Mo-, Nb- and Ta-doped rutile SnO_2. Opt Quant Electron 48:160. doi.org/10.1007/s11082-015-0287-y
[64] Bernard JE, Zunger A (1986) Optical bowing in zinc chalcogenide semiconductor alloys. Phys Rev B 34:5992–5995(R). doi.org/10.1103/PhysRevB.34.5992
[65] Cai MQ, Yin Z, Zhang MS (2003) First-principles studies of electronic, optical, and vibrational properties of $LaVO_4$ polymorphs. Appl Phys Lett 83:2805–2807. doi.org/10.1063/1.1616631
[66] Rafique M, Unar MA, Ahmed I, Chachar AR, Shuai Y (2018) First-principles calculations of six structures of alkaline-earth metal cyanide $A(CN)_2$ (A = Be, Mg, Ca, Sr, Ba): Structural, electronic, and phonon properties. J Phys Chem Solids 118:114–121. doi.org/10.1016/j.jpcs.2018.03.007
[67] Gadomska BR (1982) Influence of the interaction between dipoles, optically induced in a crystal lattice, on the nonlinear refractive index of crystals. Phys Rev B 26:1942. doi.org/10.1103/PhysRevB.26.1942
[68] Penn DR (1962) Wave-number-dependent dielectric function of semiconductors. Phys Rev 128:2093. doi.org/10.1103/PhysRev.128.2093
[69] Bekhedda K, Hiadsi S, Ziane MI, Samira K (2022) Optoelectronic study of $CuAlX_2$ (X = S, Se, Te) chalcopyrite semiconductor. Russ J Phys Chem 96:1986–1994. doi.org/10.1134/S0036024422090175
[70] Shahsafi A, Xiao Y, Salman J, Gundlach S, Wan C, Patrick J, Mikhail A (2018) Mid-infrared optics using dielectrics with refractive indices below unity. Phys Rev Applied 10:034019. doi.org/10.1103/PhysRevApplied.10.034019